Dynamics of laser-ablated MgB_2 plasma expanding in argon probed by optical emission spectroscopy

Salvatore Amoruso,[1,2] Riccardo Bruzzese,[1,3] Nicola Spinelli,[1,3] Raffaele Velotta,[1,3] Marco Vitiello,[1,3] and Xuan Wang[1]
[1]*Coherentia-INFM, Via Cintia, 26 Ed. G-80126 Napoli, Italy*
[2]*Dipartimento di Ingegneria e Fisica dell'Ambiente, Università della Basilicata, C.da Macchia Romana, 85100 Potenza, Italy*
[3]*Dipartimento di Scienze Fisiche, Università di Napoli, Via Cintia, 26 Ed. G-80126 Napoli, Italy*
(Received 1 October 2002; revised manuscript received 4 February 2003; published 10 June 2003)

We have used time and space-resolved optical emission spectroscopy to study the expansion dynamics of the plasma generated by pulsed laser ablation of solid targets of the recently discovered superconducting MgB_2 into a background Ar gas at different pressures. Our analysis clearly indicates that, above a fixed pressure, plasma propagation into Ar leads to both the formation of a shock wave, which causes a considerable increase of the fraction of excited Mg atoms, and the simultaneous reduction of the kinetic flux energy of the ablated atoms. These results have then been analyzed in the framework of a simplified gas dynamic approach for the description of free-plume self-similar expansion and of a point-blast-wave model to account for the interaction of the plume with the Ar ambient gas, thus obtaining full support and a sound physical interpretation of our experimental observations. Finally, we have related our conclusions to the general problem of the optimization of the thin-film deposition of laser-ablated materials, with particular emphasis given to the specific case of MgB_2, which is of great, present interest.

DOI: 10.1103/PhysRevB.67.224503 PACS number(s): 74.70.−b, 81.15.Fg, 52.50.Jm, 52.50.Lp

I. INTRODUCTION

The study of the expansion of material into an ambient background is an important issue of gas dynamics[1–3] and is of interest to many research disciplines such as materials research,[4,5] fluid dynamics,[2] chemical physics,[6,7] and others. In the case of pulsed laser ablation and deposition (PLD) of materials, the study of the plasma expansion dynamics into a gas environment is of fundamental importance because the quality of the deposited films is critically dependent on the range and profile of the kinetic energy and density of the ablated plume.[4,8] Consequently, the observed differences in plume dynamics when ablation occurs with and without background gases is of crucial importance and this has originated a great amount of experimental and theoretical work.[9–12] In all instances, the background gas acts as a regulator of ablated plumes energetics and strongly determines the composition and dynamical behavior of the plume material that is ablated from a solid target and deposited on a substrate. Eventually, the complex process of the plume expansion into an inert gas lends itself as a powerful means to control and optimize the film-growth process by varying key experimental parameters such as laser fluence, target-substrate distance, and nature and local pressure of an ambient gas into the deposition chamber. A clear example of this has been given in Ref. 13, where it was found that energetic components of the plume may cause damage to growing films and that this can be controlled, to a certain extent, by the pressure of an ambient gas.[14] An analytical study of this phenomenon was then given in Ref. 12.

Recently, there have been reports on *in situ* as-grown superconducting MgB_2 thin films deposited by PLD in an argon buffer gas.[15,16] The binary intermetallic compound MgB_2 has a transition temperature approaching 40 K, which makes it intermediate between the families of low- and high-temperature superconductors and potentially attractive for technological applications in the temperature range 20–30 K.[17,18] In particular, while *in situ* deposition of epitaxial MgB_2 films is required for the realization of many electronic applications, such as Josephson junctions and heterostructures, the high volatility of magnesium makes the deposition of superconducting MgB_2 thin films a quite difficult task.

The studies of Refs. 15 and 16 indicated that the ambient Ar atmosphere influences to a great extent MgB_2 laser ablation and deposition processes, and can favor, under certain experimental conditions, the deposition of superconducting thin films of good quality. Nonetheless, a clear understanding of how the background Ar pressure influences MgB_2-laser-produced plasma kinetics and dynamics at a fundamental level is still lacking.

From the perspective of controlling MgB_2-film-growth processes and in an effort to elucidate the basic physical mechanisms influencing gas phase chemistry and expansion dynamics, we have undertaken a detailed study of MgB_2 laser ablation in an Ar ambient gas. In particular, among the different techniques devised to study the plume produced during laser ablation, we have used optical emission spectroscopy, which has been proved particularly suitable for the analysis of the evolution of the plume composition and kinetics, since the emitting species are present for much longer times than their corresponding lifetimes, due to reexcitation mechanisms within the expanding plasma.[8,19,20]

We have thus carried out time- and space-resolved investigations of the emission spectrum of the plume produced by pulsed laser ablation of a MgB_2 target irradiated at different Ar ambient pressures. Our investigation was first focused on the identification of the strongest emission lines from excited species in MgB_2-laser-ablated plasmas over a broad spectral range (200–700 nm). Once the emitting species were identified, time-resolved optical spectroscopy was used to map the

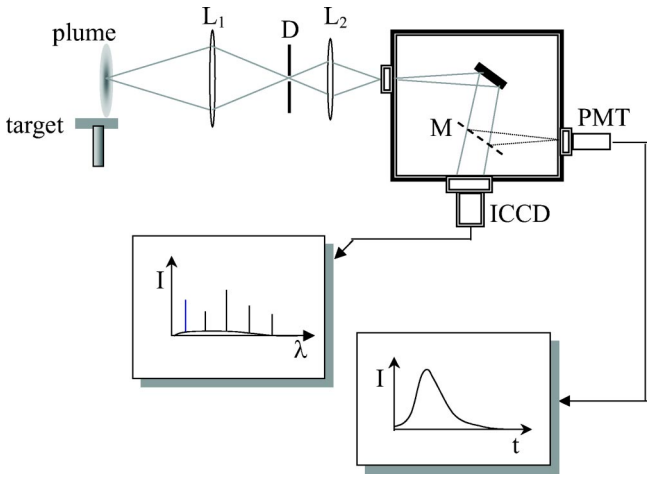

FIG. 1. Experimental setup. See text for full details.

temporal and spatial evolution of selected chemical species as a function of the ambient Ar gas pressure. We have then analyzed the experimental results by considering a simplified gas dynamical approach which makes use of energy conservation for the description of free-plume self-similar expansion, whereas a point blast wave model has been adopted to account for the interaction of the plume with the ambient gas.[21] The outcome of our spectroscopic analysis clearly indicates that, above a fixed pressure, plasma propagation into Ar leads to both the formation of a shock wave, which causes a considerable increase of the fraction of excited Mg atoms, and the simultaneous reduction of the kinetic flux energy of the ablated atoms. These results can be very usefully related to the optimization of the MgB_2-thin-film deposition process.

The approach to the description of a laser-ablated plume into a background gas we propose is particularly versatile, simple, and rapid if compared to long, *ab initio* gas dynamics numerical calculations and has the great merit of providing a much more direct physical evidence of the role played by the buffer gas. Although approximated, our analysis has produced numerical predictions which turn out to be in good agreement with features observed in actual experiments.

This paper is organized in five sections. The experimental setup and results are discussed in Secs. II and III, respectively. Section IV contains the gas dynamics modeling of the process and the comparative interpretation of the experimental findings. Finally, the summary and conclusions are given in Sec. V.

II. EXPERIMENT

A schematic of the experimental setup is shown in Fig. 1. In our experiments, a XeF excimer laser ($\lambda = 351$ nm) was used to produce ablation of a stoichiometric MgB_2 target. The laser output beam, with a pulse duration of $\approx$20 ns [full width at half maximum (FWHM)], was focused onto the MgB_2 target with a single pulse energy density of 3 J cm^{-2}. The target was mounted on a rotating holder and placed in a vacuum chamber evacuated to a residual pressure of 10^{-8} mbar. During the experiments, the chamber was filled with Ar gas and the pressure was varied in the range 10^{-4}–1 mbar.

The bright plasma emission from a selected spatial region was collected through a side window at right angles to the plume expansion direction. A system of collimating and focusing lenses (L_1 and L_2) produced a 3:1 correspondence between the sampled area of the plume and the image. Part of the plume image was selected by a $0.1(\mathrm{w})\times 8(\mathrm{h})$ mm^2 diaphragm (D) and imaged (with a spatial resolution of $\approx$300 μm) onto the entrance slit of a 0.25-m monochromator (Jobin-Yvon, HR250) equipped with a turret of two interchangeable gratings (1200 groves/mm, 100 groves/mm, maximum resolution $\approx$0.05 nm).

The plasma optical emission characterization included both spectral analysis of all the emitting species in the spectral range 200–700 nm and the time-resolved measurements of selected lines. In the first instance, the variation of the plasma emission as a function of the Ar pressure at different distances from the target surface was monitored by coupling the exit slit of the monochromator to an ICCD camera operated in the vertical binning mode of the CCD array to obtain spectral emission intensity versus wavelength. In order to record the emission spectrum in the largest wavelength range we acquired the spectra with the 100 groves/mm grating. The 1200 grooves/mm grating was then used to obtain a more reliable and fine identification of the most significant lines in the investigated spectral range. The identification of the emitting species was accomplished by standard data available in the literature.[22] The overall spectral resolution of the system in this configuration was about 0.4 nm.

In the time-resolved measurements, the monochromator was coupled, through the movable mirror (M), to a photomultiplier tube (PMT) to track the temporal evolution of selected spectral lines of excited Mg and B atoms and ions. The signal wave forms were acquired by a 500-MHz digitizing oscilloscope triggered by a fast photodiode collecting the light scattered by the laser beam focusing lens. The temporal profile of the fluorescence at a fixed distance was obtained by averaging multiple laser shots (typically 100) to improve the signal-to-noise ratio.

III. RESULTS AND DISCUSSION

In the present experiment we varied the buffer gas pressure in the range 10^{-4}–1 mbar, observing a corresponding variation in the plume color and shape, in agreement with the qualitative observations reported in Refs. 15 and 16 during *in situ* PLD of MgB_2 thin films. In particular, in our experimental conditions, a green plume was produced close to the target at an Ar pressure lower than 1×10^{-2} mbar. Then, by increasing the background gas pressure in the range 5×10^{-2}–1 mbar, a long and bright sky-blue plasma plume was observed, the plume being more confined for larger pressures. Since the concentration of the excited species in the plume is proportional to the intensity of the spectral lines, the observed changes in the plume emission can be related to the evolution of the plume composition and kinetics of the excited species in the ejected vapor.

In the following subsections the experimental results ob-

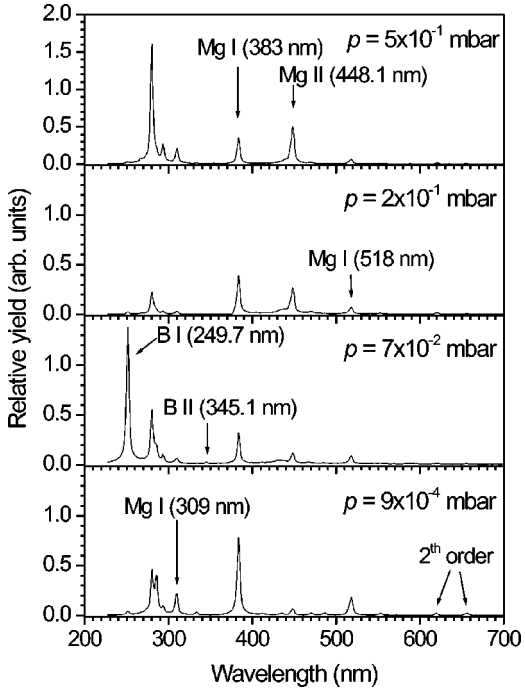

FIG. 2. Optical emission spectra of MgB_2 plume at different pressures of the Ar buffer gas, for $d=5$ mm.

tained by optical emission spectroscopy of the MgB_2 plume expanding in Ar at different background pressures and for different distances d from the target surface are presented.

A. Time-integrated emission spectroscopy

Figure 2 compares the spectra from the MgB_2 plume for different Ar background pressures at a representative distance of 5 mm from the target surface. Each spectrum has been normalized to the total collected emission light intensity registered at that pressure to provide the relative yield of the different species. The most intense Mg and B lines observed are summarized in Table I. The broad peak in the UV around 285 nm is due to the overlapping of the spectrally very close emission lines of excited B and Mg atoms and ions present in such a region, unresolved by the 100 grooves/mm grating.

The spectra mainly consist of neutral B and Mg lines (B I and Mg I), with some contributions from their excited ions (B II and Mg II), and the plume emission in the visible range

TABLE I. Electronic transition, lifetime τ, wavelength λ, and species of the emission lines used in this study.

Species	λ (nm)	Configuration	τ (ns)
B I	249.7	$2s^2 3s\ ^2S$-$2s2p\ ^2P^0$	2.8
Mg I	285	$3s5d\ ^3D$-$3s3p\ ^3P^0$	12.3
		$3s5d\ ^1D^0$-$3s^2\ ^1S$	2.0
Mg I	309	$3s4d\ ^3D$-$3s3p\ ^3P^0$	5.9
Mg I	383	$3s3d\ ^3D$-$3s3p\ ^3P^0$	2.4
Mg II	448.1	$4f\ ^2F^0$-$3d\ ^2D^0$	2.2
Mg I	517	$3s4s\ ^3S$-$3s3p\ ^3P^0$	9.6

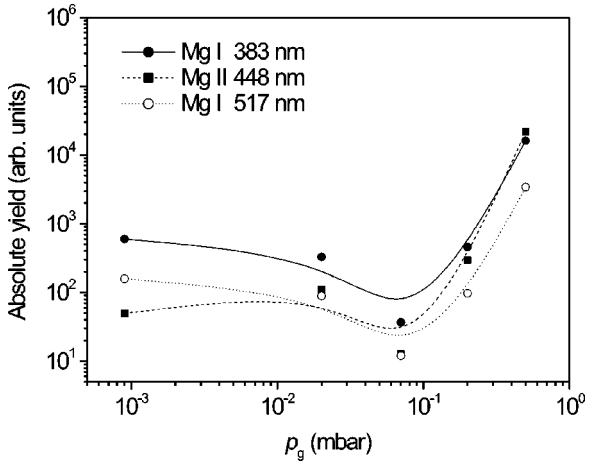

FIG. 3. Yields of Mg atoms and ions as a function of the Ar background pressure at a distance $d=5$ mm from the target surface. The lines are a guide for the eye.

can be mainly ascribed to Mg I and Mg II. In particular, while at low buffer pressure (up to $\approx 10^{-1}$ mbar) the contribution from the Mg I 517 nm ($3s4s\ ^3S$-$3s3p\ ^3P^0$) green line to the emitted visible light is larger than that of the Mg II blue line at 448.1 nm ($4f\ ^2F^0$-$3d\ ^2D$), this last line strongly increases as the buffer gas pressure grows up, becoming almost an order of magnitude larger than the green line at the larger pressures. Thus this feature fully accounts for the change in color of the plume emission as a function of the Ar pressure.

Another interesting feature of the spectra of Fig. 2 is the absence of any sizable emission ascribable to molecular bands, which rules out a significant presence of molecular compounds in the plume. Thus the variation of the plume emission as a function of the Ar background pressure can be totally related to excitation and ionization mechanisms involving the elemental species which contribute to the visible plume.

In Fig. 3 the yield of the Mg excited atoms and ions as a function of the Ar background pressure is reported, at a distance of 5 mm from the target surface. We observe that both Mg I and Mg II yields show a steep increase above a pressure of $\approx 7\times 10^{-2}$ mbar, indicating the presence of a mechanism promoting excitation and ionization of the Mg species above such a pressure. This highlights the significant role played by the Ar buffer in determining the plasma dynamics by influencing the excitation and ionization equilibrium between different excited species.

B. Time-resolved measurements

To better elucidate the plume dynamics in an Ar environment by discriminating between the possible different mechanisms at a fundamental level (such as collisional excitation and ionization, plume heating, etc.) responsible for the increase in the atomic excitation observed at higher Ar pressures, the evolution of selected species was analyzed by time-resolved optical spectroscopy. In the following the experimental results relative to B I (249.7 nm), Mg I (383 nm), and Mg II (448.1 nm) lines are reported.

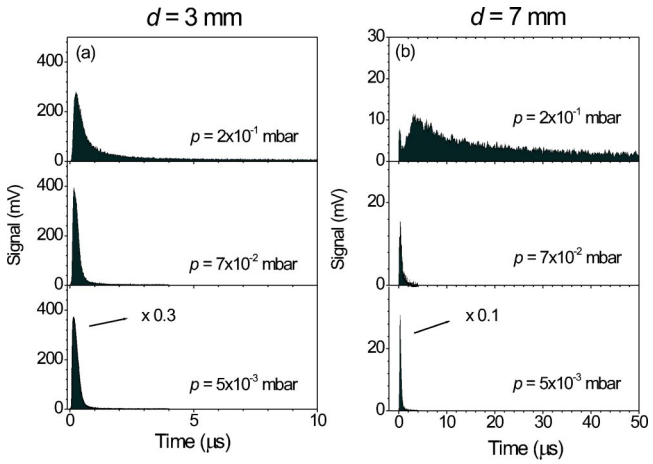

FIG. 4. Emission intensity temporal profile of the Mg I atoms at 383 nm at various Ar pressures and for two distances d from the target surface: (a) $d=3$ mm and (b) $d=7$ mm.

In Figs. 4 and 5 the emission intensity temporal profiles obtained from the Mg I 383 nm and B I 249.7 nm lines, respectively, observed at two different distances (3 and 7 mm) from the target surface are shown. The temporal features observed for the 383 nm Mg I line are quite similar to that observed for other Mg I spectral lines.

In Fig. 4(a) the spectral emission of Mg I at 3 mm from the target surface shows the appearance of a considerable tail at longer times by increasing the pressure from 5×10^{-3} to 2×10^{-1} mbar. A similar behavior is observed for $d=7$ mm (b), with the emission tail extending up to $\approx$70 μs at 2×10^{-1} mbar. Similar findings can be observed in Fig. 5 for B atoms, although the long tail in the emission intensity appears at slightly larger background pressures ($\geqslant$0.5 mbar).

Figure 6 shows the spectral emission profile from the 448.1 nm Mg II line for two different distances from the target surface, at a pressure of 2×10^{-1} mbar. Also for this species, by passing from 3 to 7 mm, we can appreciate the appearance of a delayed component in the emission intensity distribution.

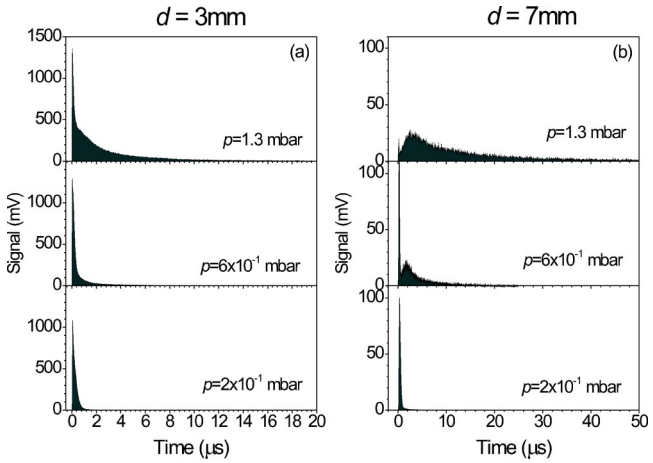

FIG. 5. Emission intensity temporal profile of the B I atoms at 249.7 nm at various Ar pressures and for two different distances d from the target surface: (a) $d=3$ mm and (b) $d=7$ mm.

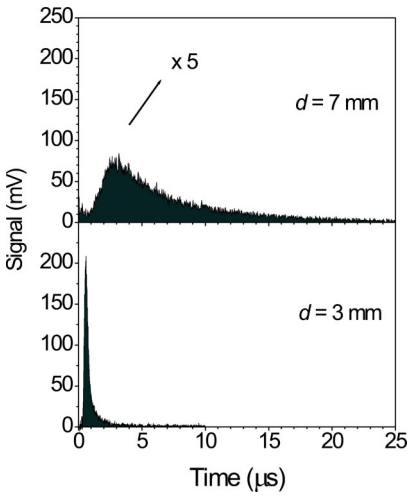

FIG. 6. Emission intensity temporal profile of the Mg II atoms at 448.1 nm at two different distances d from the target surface for an Ar background pressure of 2×10^{-1} mbar.

In Fig. 7 we report the integrated emission yield of Mg I (383 nm) and Mg II (448.1 nm) as a function of the distance d from the target at different Ar background pressures. The integrated yield, obtained by considering the whole area under the emission profile, gives an indication of the amount of excited species which will be deposited on a substrate located at a distance d from the target surface. We observe an increase in the excitation of both the Mg atoms and ions as the pressure increases. In particular, at an Ar pressure of 2×10^{-1} mbar the emission signal due to the 383 nm Mg I line [Fig. 7(a)] registered at larger distances from the target is considerably bigger than that relative to 5×10^{-3} mbar. A similar behavior is followed by the 448.1 nm Mg II line [Fig. 7(b)]. This observation is in good agreement with the data obtained by time-integrated optical emission spectroscopy and reported in Fig. 3, and clearly shows that the Ar gas environment strongly affects the population kinetics of Mg

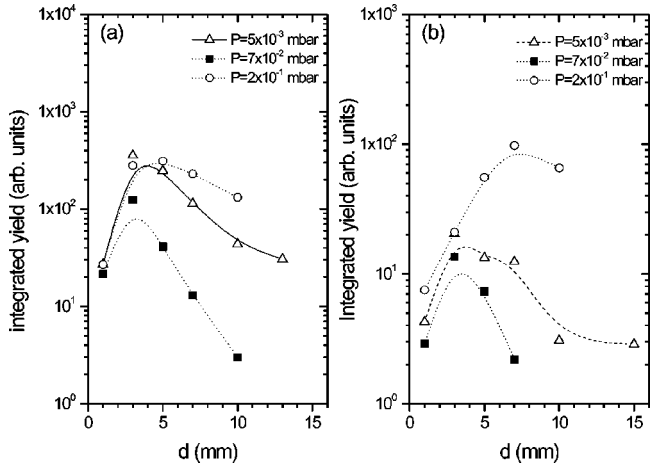

FIG. 7. Integrated emission line intensity as a function of the distance d from the target surface for different Ar pressures: (a) 383 nm Mg I line and (b) 448.1 nm Mg II line. The lines are a guide to the eye.

TABLE II. Average values of the mean free paths for the observed species in the plume at the different Ar pressures investigated.

	Mean free paths (mm)			
p_g (mbar)	Mg I	B I	Mg II	B II
5×10^{-3}	38	69	89	191
7×10^{-2}	2.7	4.9	6.3	14
2×10^{-1}	0.95	1.7	2.2	4.8
6×10^{-1}	0.32	0.57	0.7	1.6
1.3	0.15	0.26	0.3	0.73

atoms and ions for pressures of $\approx10^{-1}$ mbar at distances of some mm from the target surface.

The integrated yield of the 249.7 nm B I line is shown to be only slightly influenced by the Ar buffer gas at all the pressures investigated. This different behavior of the 249.7 nm B I line with respect to the investigated Mg spectral lines can be ascribed both to the longer mean free path of B atoms in Ar buffer gas with respect to Mg (see Table II) and to radiation trapping effects as the corresponding transition is coupled to the ground state.

C. Plume expansion in a background gas

In ns laser ablation, the evaporation of material is due to a high initial heating rate, which mainly produces a neutral vapor. The subsequent coupling of the laser pulse with this nascent vapor results also in extensive ionization of the ablated material and free-electron production.[8,23] Therefore, the plasma plume consists of ions, electrons, and neutrals. The ions have, typically, higher kinetic energies than neutrals, since their expansion is influenced by space-charge effects in addition to pressure gradients. Nevertheless, the presence of energetic neutrals in the plume is also observed due to the recombination of energetic ions.

The collisional dynamics taking place during plume expansion into the background gas also affects the plume chemical kinetics. In this respect, it is worth reporting that the mean free path of the emitted atoms—Mg, for instance—with kinetic energies of several tens of eV in an Ar background scales from few tens of cm at 10^{-3} mbar to few mm at 10^{-1} mbar and to tenths of mm at 1 mbar (see Table II), as estimated by using the equations reported by Westwood.[24] Thus, in our experimental conditions, the expansion dynamics of the ejected species is influenced by collisions with the buffer gas atoms on propagation distances of the order of a few mm for Ar pressures in the range 10^{-1}–1 mbar.

In our experiment, we observe a revival of excitation and ionization of the plume species at larger pressures, as reported in Figs. 3 and 7. Since the lifetime of the excited states investigated, reported in Table I, is always of the order of tens of ns, the observed increase of optical emission intensity can only be due to processes occurring during plume expansion. These processes lead to a transfer of energy from direct motion to internal degrees of freedom of the expanding particles, influencing the plume population kinetics. The energy transfer can basically occur through shock-wave (SW) formation and consequent plume heating and inelastic collisions with buffer gas atoms. Such mechanisms will be briefly analyzed below.

Shock waves have been widely employed in the description of plume expansion into an ambient gas.[4,10,25,26] The formation of a SW—and the consequent plume heating—depends critically on a number of factors such as molecular weight of plume and background species, ambient gas pressure, initial plume velocity, and density. In typical PLD conditions the plume expands at supersonic speed and the ablation rate is usually high enough for SW formation at ambient pressures of the order of 0.1–1 mbar, as observed by different authors for various experimental conditions.[25–28] Moreover, experiments and simulations on Si (whose mass and radius are close to that of Mg) in Ar have shown that just few collisions are necessary to slow down the plume, thereby leading to a shock wave at background pressures of the order of $\approx$0.1 mbar.[12]

Position-time plots of the leading edge of the plume emission and of the emission intensity maximum have been largely used to investigate PLD plume propagation into an ambient gas in the presence of a SW,[10,25–28] although, in reality, the temperature increase behind the shock front changes the population of the excited states of atomic species. In fact, the emission intensity $I(d)$ is related to the density of the plume atoms, $\rho(d)$, through the relation

$$I(d)\propto\rho(d)\exp-\frac{E_u}{k_BT(d)}, \tag{1}$$

where $T(d)$ is the temperature at the distance d from the target and E_u is the energy of the upper level of the optical transition. Since in a SW ρ increases going from the plume center to the front, whereas T is a decreasing function of d, from Eq. (1) it follows that the emission maximum does not coincide with the shock front; rather, it is located behind it.[29] Although a rigorous analysis of such an effect would require a very complex modeling of the plume dynamics, we can estimate the difference between the actual position of the shock front R and the distance d_M at which maximum emission intensity I_M is detected by considering the simplified case of an ideal spherical point blast wave undergoing a self-similar expansion. In this last case, by using the density and temperature profile for a monoatomic gas,[21] shown in Fig. 8(a), and assuming $E_u\approx6$ eV, as is the case for the 383 nm Mg transition, we obtain the intensity emission distribution reported in Fig. 8(b). This figure clearly shows that even at a temperature as low as 0.5 eV the position of the emission intensity maximum d_M is only shifted by a factor $\epsilon\approx0.1$ with respect to the shock-front position. As discussed in the following section, a temperature of the order of 1 eV is a reasonable estimation in the conditions of our experiment, thus leading to $\epsilon\approx0.05$. Since our optical emission measurements have been carried out at distances from the target of the order of some mm (typically 3–7 mm), an actual spatial shift between the observed emission intensity maximum and the shock front of only ≈300 μm can be inferred.

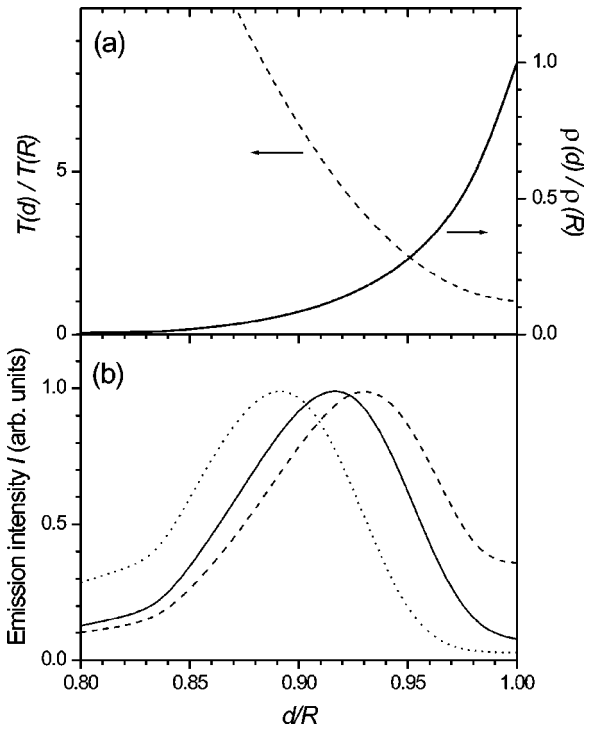

FIG. 8. (a) Temperature and density profile for an ideal point blast wave (Ref. 21) and (b) emission intensity profile derived from Eq. (1) for three different temperatures $T(R)$ at the shock front R: $T(R)=0.5$ eV (dotted line), $T(R)=1.0$ eV (solid line), and $T(R)=1.5$ eV (dashed line), in the case of an ideal point blast wave. The arrow indicates the flow of time at a fixed distance d.

Owing to the above reported considerations, there will be a delay Δt between the instant at which the shock front reaches the distance d, t_R, and the instant at which the maximum in the emission intensity temporal profile is observed with respect to the laser pulse, t_M. This delay Δt can be approximately worked out in the ideal case of a spherical point blast wave,[21] when the relation between the distance of the shock front from the point of explosion, $R(t)$, and the time t is of the kind $R(t) \propto t^{2/5}$ (see Refs. 21 and 30). As previously discussed, when moving from the shock front inward, the maximum emission intensity is found after a distance of the order of $\epsilon R(t)$, and this distance has been traveled by the SW at a speed $\approx \dot{R}(t)$. Thus,

$$\Delta t \approx \frac{\epsilon R}{\dot{R}} = \frac{5}{2}\epsilon t_R, \tag{2}$$

which leads to

$$t_M \approx \left(1+\frac{5}{2}\epsilon\right) t_R. \tag{3}$$

Although obtained in the case of an ideal point blast wave, Eq. (3) highlights both the direct proportionality between t_R and t_M and that $(\Delta t/t_R)$ is typically pretty small (≈ 0.1, for $\epsilon=0.05$). This makes the emission intensity maximum a reliable parameter to investigate the plume dynamics in background gas.[10,28]

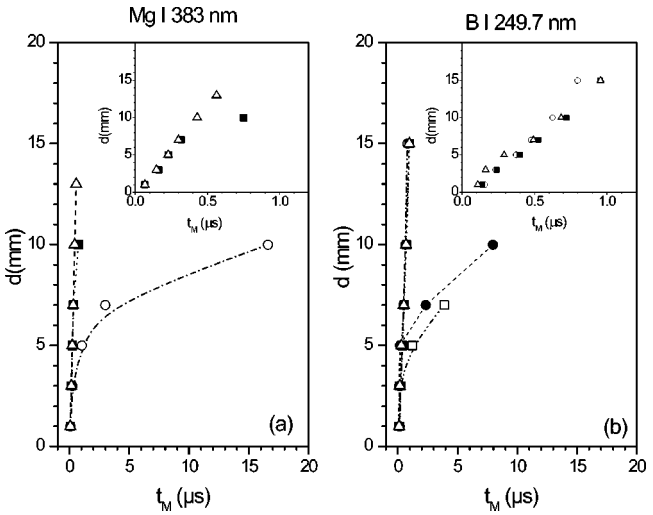

FIG. 9. Distance d from the target vs time t_M at which the maximum in the emission intensity profile is observed, for the (a) Mg I 383 nm line and (b) B I 249.7 nm line, at different Ar pressures: (open triangles) $p_g=5\times10^{-3}$ mbar, (solid squares) $p_g=7\times10^{-2}$ mbar, (open circles) $p_g=2\times10^{-1}$ mbar, (open squares) $p_g=6\times10^{-1}$ mbar, and (solid circles) $p_g=5\times10^{-1}$ mbar. The insets show an enlarged view of the first μs.

D. Effects of collisions

In Figs. 9(a) and 9(b) the dependence of the distance d from the target on the time t_M at which the maximum in the emission intensity temporal profile is observed with respect to the laser pulse is shown, for different Ar pressures, for both Mg I and B I. For the Mg I emission line the results obtained at pressures smaller than 10^{-1} mbar show an almost linear dependence over the whole range of distances for which emission could be detected (triangles and solid squares), as shown in the inset of Fig. 9(a) where the time interval 0–1 μs has been magnified for clarity. On the contrary, when the Ar pressures exceed $\approx 10^{-1}$ mbar (open circles), the dependence is no longer linear for d larger than 3 mm. Similar features were observed for the other Mg emission lines studied. The velocities obtained from the slope (d/t_M) in the linear region are $\approx 2\times10^6$ cm/s for Mg neutrals and $\approx 3.0\times10^6$ cm/s for Mg ions. The behavior observed at larger pressures is, thus, consistent with the presence of a slowing down effect on these atoms by the ambient atmosphere, as also reported by other authors.[10,26–28]

For the B I emission line [see Fig. 9(b) and inset], the velocity in the linear region is $\approx 1.5\times10^6$ cm/s, while the braking effect of the ambient atmosphere is not observed until a pressure of about 6×10^{-1} mbar is reached, and at distances of about 5 mm, consistent with the longer mean free path of B atoms in Ar background gas.

Then, we observe a sharp increase of t_M at larger pressures and distances (the slope of the d-t_M curve decreases), which constitutes a clear indication of a slowing down of the plasma expansion dynamics with respect to the free-expansion behavior registered at low pressures and short distances.

The sharp increase of t_M above a certain distance at larger pressures is consistent with a shock-wave-like dynamics just

in the region where the revival of excitation is observed. In fact, the formation of a shock wave produces a redistribution of kinetic and thermal energy between the plume and the ambient gas, resulting in a significant transformation of particles flux velocity into plume thermal energy. This leads to the heating of the plume with the consequent revival of excited species populations experimentally observed.

Actually, even inelastic collisions between atoms could produce excitation and ionization of one or both colliding particles. In particular, for a head-on collision between an atom of mass M_c traveling with a kinetic energy E_k and a stationary particle of mass M_g, the maximum fraction of energy f which can be transferred from the atom into internal energy of either colliding species is given by

$$f=\frac{\Delta E_k}{E_k}=\frac{M_g}{M_c+M_g}, \tag{4}$$

which, for instance, in a collision between Mg and Ar, leads to $f\approx 62\%$. Since the energy required for Ar excitation and ionization is quite larger than the excitation and ionization energy of Mg, collisional-induced excitation and ionization of Mg are more probable than for Ar by this mechanism. Nevertheless, given the rapid slowing down of the plume atoms observed in Fig. 9, although inelastic collisions could be of importance at small distances from the target, they cannot explain the excitation and ionization revival observed at larger distances from the target surface for high background pressures. In fact, at several mm from the target surface, where we observe a maximum in the degree of excitation for Mg [see Fig. 8(b)], the plume slowing down effect reduces the particles kinetic energy to values at which collision-induced excitation and ionization are not effective anymore. This is due to the large number of collisions with the background gas atoms, as evidenced by the small average mean free path at high pressures (see Table II).

IV. GAS DYNAMICS OF PLUME EXPANSION AND SHOCK-WAVE FORMATION

In PLD energetic particles are generated close to the target and are accelerated away from the surface by pressure gradients. In high-vacuum conditions and when the particle mean free path is larger than the characteristic length of the experiment, the plasma plume expands adiabatically and fast reaches an inertial stage, where almost all energy deposited in the produced plume is transformed in kinetic energy (*free plume*). An analysis of this regime can be obtained by using self-similar profiles of plume thermodynamic variables satisfying gasdynamics equations under the condition of energy conservation.[21,31] On the other hand, the hydrodynamics of laser-produced plasma expansion in background gases has been modeled in different ways, depending on the pressure range. For the early stages and at low pressures the scattering of ablated species by gas atoms is usually described in terms of a viscous effect.[4] At high pressures, when the mean free path of the expanding particles is low enough for different collisions to occur, the formation of SW's has been experimentally observed[4,10] and theoretically modeled.[32]

A simplified analysis of the free-plume regime can be obtained by considering the conservation of energy (thermal plus kinetic) for a hemispherical plume expansion. In this case, the density ρ_p and pressure p_p profiles, which satisfy the equations of gasdynamics, for a monoatomic gas (namely, heat capacity ratio $\gamma=5/3$), are given by[31,32]

$$\rho_p(r,R)=\frac{16M_p}{\pi^2R^3}\left[1-\left(\frac{r}{R}\right)^2\right]^{3/2}, \tag{5}$$

$$p_p(r,R)=\frac{256E_p}{15\pi^2R_0^3}\left(\frac{R_0}{R}\right)^5\left[1-\left(\frac{r}{R}\right)^2\right]^{5/2}, \tag{6}$$

with the velocity profile inside the plume expressed as

$$v_p(r)=r\frac{\dot{R}(t)}{R(t)}, \tag{7}$$

where r is the radial coordinate, M_p and E_p the mass and energy of the plume, and R_0 and R the plume radii before expansion and at time t, respectively. Equations (5) and (6) have been obtained by considering that the hemisperical case can be derived from the spherical expansion equation by using the doubled energy and mass of the plume.[31,32]

As the initial plume radius R_0 is of the order of the laser waist on target—i.e., a few tens of microns—the conservation of energy is given by

$$E_p=E_k+E_{\rm th}=\frac{1}{2}\int_{R_0\approx 0}^{R(t)}\rho_p(r,R)v_p^2(r,R)2\pi r^2dr + \frac{3}{2}\int_{R_0\approx 0}^{R(t)}p_p(r,R)2\pi r^2dr, \tag{8}$$

where E_k and $E_{\rm th}$ are the kinetic and thermal plume energies, respectively. By using Eqs. (5) and (6), expression (8) takes the form

$$E_p=\tfrac{3}{16}M_p\ddot{R}^2+E_p\left(\frac{R_0}{R}\right)^2. \tag{9}$$

After a short time, the plume expands inertially and R becomes much larger than R_0. Then the thermal energy $E_{\rm th}$ becomes much less than the kinetic energy E_k, leading to

$$E_p\approx\tfrac{3}{16}M_p\dot{R}^2=\tfrac{3}{16}M_pv_f^2, \tag{10}$$

v_f being the plume expansion velocity in the inertial stage. This result shows that the plume expansion velocity in vacuum can be related to the ablated mass and to the energy initially stored in the nascent plasma. For instance, in our experimental conditions, the release of a few nanograms of material, at an irradiation energy of a few mJ, leads to plume velocities of the order of 10^6 cm/s, as indeed observed.

A rigorous treatment of plasma plume expansion in a buffer gas and, above a certain pressure, shock-wave formation requires a more complex modeling and numerical analysis with respect to the free plume. Therefore, instead of using numerical approaches, one can consider a simplified analysis based on analytical expressions for shock-wave formation and dynamics. In particular, point-blast-wave (PBW) equa-

tions have been largely employed to describe the plume expansion into a buffer gas.[4,10,21,32] According to the PBW model, the relation between the position of the shock front from the point of explosion R and the time t is expressed as[30]

$$R(t)=\left(\frac{\alpha E}{\rho_g}\right)^{1/(n+2)} t^{2/(n+2)}, \tag{11}$$

where E is the energy released in the explosion and ρ_g is the density of the undisturbed buffer gas, while n and α are parameters assuming the values $n=3$, 2, and 1 and $\alpha=1.175$, 1.015, and 1.845 for spherical-, cylindrical-, and plane-wave propagation, respectively. In particular, E is an energy, an energy per unit length, and an energy per unit area for spherical, cylindrical, and planar propagation, respectively.

We point out that the initial ablated particles provide the energy for the shock-wave generation through collisions with the ambient gas atoms, which finally lead to plume thermalization. Thus, the particle energy distribution becomes more and more isotropic, giving rise to the approximately hemispherical behavior of the shock-wave propagation observed in a number of PLD experiments[25,26,33] and considered in theoretical modeling.[32] In the case of hemispherical expansion, Eq. (11) can be rewritten in terms of the blast-wave energy released in the explosion E, which as usual can be assumed equal to 2 times the hemispherically expanding plume energy E_p, and the background gas pressure p_g, as

$$R(t)=\xi\left(\frac{E_p}{p_g}\right)^{1/5}(c_g t)^{2/5}, \tag{12}$$

where ξ is a dimensionless constant, which for $\gamma=5/3$ assumes a value of ≈ 1, and c_g is the sound speed in the undisturbed buffer gas.

In the SW regime, the high-pressure expanding plume compresses the surrounding buffer gas acting as a piston. The adjoint mass of the ambient gas at the plume periphery produces a braking effect on the expanding particles, resulting in large deviations with respect to the free expansion when the mass (pressure) of the gas surrounding the leading edge of the plume is comparable with the plume mass (pressure) itself.[21] Thus a distance-related pressure threshold exists for plume slowing down. Assuming a hemispherical expansion of the plume, an approximate distance-related pressure relation can be derived by this condition: namely,

$$\tfrac{2}{3}\,\pi R_{\mathrm{SW}}^2 \rho_g \approx M_p, \tag{13}$$

R_{SW} being the distance above which a shock wave is formed at the background density ρ_g. By using Eq. (10), the condition (13) can be reexpressed in terms of the buffer gas pressure p_g:

$$R_{\mathrm{SW}}\left(\frac{E_p}{p_g}\right)^{-1/3} \approx \left(\frac{8}{\gamma\pi}\right)^{1/3}\left[\frac{v_f}{c_g}\right]^{-2/3}. \tag{14}$$

This shows that in the dimensionless variable $\delta=R(E_p/p_g)^{-1/3}$, the shock-wave formation starts at a point which depends on the ratio between the free-plume flux velocity v_f and the sound speed in the buffer gas, c_g. Moreover, by introducing the dimensionless time variable $\tau=tc_g(E_p/p_g)^{-1/3}$, the PBW expansion is described by

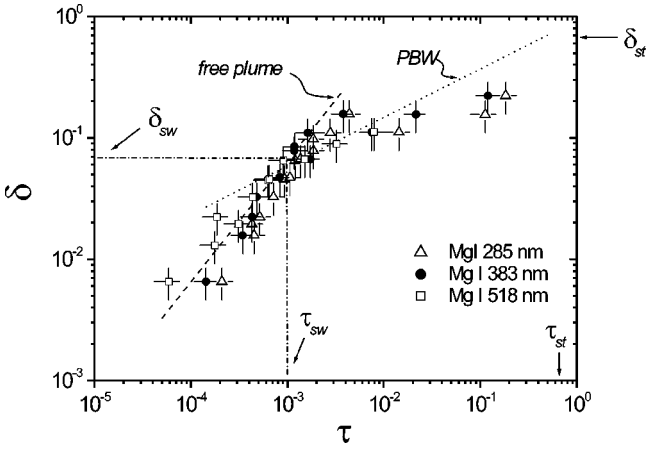

FIG. 10. Distance-time plot of the Mg I experimental data in dimensionless variables. The dotted lines describing the free-plume [Eq. (15)] and blast-wave [Eq. (16)] dynamics in our experimental conditions are also shown. The dashed horizontal and vertical lines show the point where the transition to the PBW regime takes place. The arrows indicate the values corresponding to plume stopping.

$$\delta \approx \xi\tau^{2/5}, \tag{15}$$

while the free-plume dynamics is given by

$$\delta=\left(\frac{v_f}{c_g}\right)\tau \approx \chi\tau. \tag{16}$$

In our case, we observe $v_f=(2.1\pm 0.1)\times 10^6$ cm/s, leading to $\chi\approx 65$ and to the following conditions for SW formation in dimensionless variables:

$$\delta_{\mathrm{SW}}\approx 7\times 10^{-2},$$

$$\tau_{\mathrm{SW}}=[(v_f/c_g)^{-1}\times\delta_{\mathrm{SW}}]\approx 1\times 10^{-3}, \tag{17}$$

for $\gamma\approx 5/3$. In our experimental condition, a transition to a braking regime above a distance $d\approx 4$ mm for an Ar pressure $p_g\approx 10^{-1}$ mbar is observed. Plugging these experimental values into Eqs. (13) and (10) leads to a plume energy $E_p\approx 1.8$ mJ and to an ablated mass $M_p\approx 20$ ng, respectively. These values have been used to compare the experimentally observed distance-time relations discussed in Sec. III to the analytical plume dynamics expressed in terms of the dimensionless variables δ-τ of Eqs. (15) and (16).

Figure 10 shows the δ-τ plot obtained from the data of different Mg lines. The data clearly show that initially the plume follows a free expansion [Eq. (16)], then enters a blast-wave regime [Eq. (15)] for $\delta\geqslant\delta_{\mathrm{SW}}$ and $\tau\geqslant\tau_{\mathrm{SW}}$. At the beginning of this stage the compressed ambient gas is heated and an external shock wave forms. In this respect it is worth noting that such a regime persists until the produced SW remains strong: i.e., the plume energy (thermal plus kinetic) is comparable with the energy transferred to the surrounding

compressed gas, and the plume boundary and the surrounding gas travel close to each other.

At the same time, the compressed buffer gas heats up the expanding plume to a temperature higher than that of free-plume expansion. The heating up of the plume results in the enhancement of the excitation and ionization experimentally observed at larger Ar pressures and longer distances from the target surface, as discussed in Secs. III and IV. The heating of the plume starts near the contact surface, where collisions between plume particles and buffer gas atoms occur. Subsequently, while the plume kinetic energy decreases, the external shock wave detaches from the plume boundary and degenerates into a sound wave. Then, when almost all the energy initially stored in the plume is converted in a sound wave propagating into the buffer gas, the hydrodynamic motion of the plume stops and the plume atoms thermalize with the ambient gas. At this stage, the motion of the ablated particles proceeds as a random walk into the ambient gas (diffusion). This regime (*plume stopping*) starts above a distance R_{st} such that the following condition is satisfied:

$$\tfrac{2}{3}\,\pi R_{st}^3 \rho_g c_g^2 \approx E_p\,, \tag{18}$$

which in dimensionless variables reads

$$\delta_{st} = \tau_{st} = \left(\frac{3}{2\gamma\pi}\right)^{1/3} \approx 0.66. \tag{19}$$

The plume stopping regime lower limits δ_{st} and τ_{st} have been indicated in Fig. 10 by arrows. Before the plume stopping regime is reached, the plume dynamics changes from the PBW behavior ($\delta \propto \tau^{2/5}$) to a different time dependence with the exponent decreasing from 2/5 to 0, a value which corresponds to plume stopping. This further slowing down of the plume can be observed in Fig. 10 for τ larger than $\approx 10^{-2}$ and before the plume stopping regime is reached. It is worth stressing the satisfactory agreement between the experimental data and the theoretical lines describing the plume expansion in the free-plume and PBW regimes, as well as between the theoretical and experimental values corresponding to the transition between the two dynamic regimes. This represents a key point of the physical interpretation of plume expansion in a background gas, in typical PLD experimental conditions.

The significant increase of the plume internal energy evidenced by the larger amount of excited and ionized species shown in Figs. 3 and 7, which is due to SW formation and consequent plume heating, can be discussed by considering the properties of the shocked region as representative of the compressed plume-gas system. For a strong shock, the compressed front of the blast wave has a temperature T_{SW}, a density ρ_{SW}, and a thickness ΔR, respectively, given by[21]

$$T_{SW} = \frac{2\gamma}{\gamma+1}\left[\frac{\gamma-1}{\gamma+1}M^2 + 1\right] T_g\,, \tag{20}$$

$$\rho_{SW} = \frac{\gamma+1}{\gamma-1}\,\rho_g\,, \tag{21}$$

$$\Delta R = R\,\frac{\gamma-1}{3(\gamma+1)}, \tag{22}$$

M being the Mach number, T_g and ρ_g the temperature and density of the undisturbed gas, and R the position of the shock front for a spherical propagation, respectively. In the dimensionless variables of Eq. (15), the Mach number corresponds to $\dot{\delta}(\tau) = \dot{R}/c_g$.

From Eq. (20) an estimate of the order of magnitude of the temperature in the shocked region can be obtained. In our experimental condition, we observe a Mach number M as high as 25 in the free-plume–shock-wave transition ($\tau = \tau_{SW}$), which rapidly decreases at later times. With $\gamma = 5/3$, we obtain an average temperature $\langle T_{SW} \rangle \approx 1$ eV in the region of strong SW ($10^{-3} \leqslant \tau \leqslant 10^{-2}$, in Fig. 10). Such a temperature is much higher than the free-plume temperature at the same distance from the target (typically a few tenths of eV,[34,35]) thus evidencing a significant plume heating. This leads to a degree of excitation and ionization comparable with that typically obtained at the end of the laser pulse close to the target. Moreover, the shocked region has a density of the order of $\approx$4 times that of the undisturbed gas, which, for $p_g \approx 10^{-1}$ mbar, leads to $\rho_{SW} \approx 10^{16}$–$10^{17}$ particles cm^{-3}. At this density and temperature, the degree of excitation and ionization results from the balancing between electron impact ionization and excitation and radiative recombination processes (coronal equilibrium).[36] As an example, if we consider a hydrogenlike behavior of the Mg atoms, such a balance would lead to a degree of ionization of $\approx$10%, i.e., much larger than that present at the same distances in high vacuum or low background pressures. This explains the increase of more than an order of magnitude of the Mg II emission line observed in Fig. 2 by increasing the buffer gas pressure from $p_g \approx 10^{-3}$ mbar to $p_g \approx 0.5$ mbar, as well as the large reexcitation of neutral species.

Finally, since the excitation state and kinetic energy of an impinging atom greatly influence the process of thin-film formation, the mechanisms we have observed can be of importance for the deposition of superconducting as-grown MgB_2 films, as well as of other materials. In fact, energetic particles can cause resputtering largely influencing the growing film stoichiometry, especially for the most volatile elements, like Mg in MgB_2.[11] Thus, while the slowing down effect of the ambient gas contributes to reduce the release of Mg from the deposit, the arrival of a larger extent of excited and ionized species on the growing film enhances surface atomic mobility, thus favoring thin-film growth at lower substrate temperatures, due to an increase of the thermal energy released in the impact region.

In particular, the distance-related pressure threshold reported in Eq. (14) for SW formation shows that the same behavior will occur at larger distances from target for lower Ar buffer pressures, if the SW formation conditions are fulfilled. Then, for different target-to-substrate distance values a buffer gas pressure interval optimizing the amount of plume atoms arriving on the substrate with a higher degree of internal excitation energy and a lower kinetic flux energy can be found. This observation is in fairly good agreement with the experimental findings of Ref. 16 where deposition of as-

grown MgB_2 superconducting thin films was successfully obtained only for Ar buffer pressures of the order of a few times 10^{-2} mbar, with a target-to-substrate distance of $\approx$15 mm, at laser fluences comparable to that used in the present work. Moreover, in such experimental conditions a blue plume was formed, in agreement with the results that the as-grown superconductive MgB_2 films are deposited when a shock wave develops during the plume expansion in the Ar buffer gas. In this respect it is worth observing that, considering constant all other parameters except R and p_g, Eq. (14) predicts a target-to-substrate distance of the order of 3 times that at which we observe shock-wave formation and plume excitation and ionization in our experimental conditions, when passing from a few tenths of mbar to $p_g \approx 10^{-2}$ mbar, a value which is in a fairly good agreement with the deposition condition reported in Ref. 16.

V. CONCLUSIONS

Time- and space-resolved optical emission spectroscopy has allowed us to study the expansion dynamics of laser plumes ablated from MgB_2 solid targets into an ambient Ar buffer at different pressures. Our experimental results have clearly highlighted the influence of the background Ar gas pressure on both plume kinetics and dynamics. We have observed a strong increase in the degree of excitation of Mg atoms and ions at Ar pressures higher than about 10^{-1} mbar. This increase, which is coupled to a slowing down effect of the ambient gas which drastically reduces the flux velocity of plume atoms, has been related to the formation of a shock wave causing a considerable plasma heating.

We have analyzed our findings in the frame of a simplified gas dynamic approach for the description of free-plume self-similar expansion and of a point-blast-wave model to account for the interaction of the plume with the Ar ambient gas, thus obtaining full support and a sound physical interpretation of the experimental observations. Since the excitation state and kinetic energy of an impinging atom greatly influence the process of thin-film formation, the mechanisms we have observed and their physical interpretation bear significant consequences to the problem of the optimization of the deposition process. Although approximated, our approach has produced numerical predictions which turn out to be in very good qualitative and quantitative agreement with features observed in the actual experiment. Beyond its simplicity, our method has the merit of evidencing the physical role of the quantities involved in the process and has allowed us to obtain a very reasonable estimation of pressures and distances values at which the free plume generates a shock wave or it is stopped.

In fact, the suggestions put forward by our analysis in terms of optimal background gas pressures and target-to-substrate distances are in good qualitative and quantitative agreement with recent works where deposition of as-grown MgB_2 superconducting thin films was successfully obtained only for Ar buffer pressures of the order of a few times 10^{-2} mbar, with target-to-substrate distances of about 15 mm (see Refs. 15 and 16, for example).

ACKNOWLEDGMENT

The authors are grateful to N. Arnold for valuable discussions.

[1] M. A. Liberman and A. L. Velikovich, *Physics of Shock Waves in Gases and Plasmas* (Springer-Verlag, Berlin, 1986).
[2] Yu. I. Koptev, *Gas Dynamics* (Nova, New York, 1992).
[3] R. F. Wood, K. R. Chen, J. N. Leboeuf, A. A. Puretzky, and D. B. Geohegan, Phys. Rev. Lett. **79**, 1571 (1997).
[4] D. B. Geohegan, in *Pulsed Laser Deposition of Thin Film*, edited by D. B. Chrisey and G. K. Hubler (Wiley, New York, 1994).
[5] R. Kelly and A. Miotello, Appl. Surf. Sci. **96–98**, 205 (1996).
[6] X. Wang, S. Amoruso, R. Bruzzese, N. Spinelli, A. Tortora, R. Velotta, C. Ferdeghini, G. Grassano, and W. Ramadan, Chem. Phys. Lett. **353**, 1 (2002).
[7] H. Nishikawa, M. Kanai, G. Szabo, and T. Kawai, Phys. Rev. B **61**, 967 (2000).
[8] S. Amoruso, R. Bruzzese, N. Spinelli, and R. Velotta, J. Phys. B **32**, R131 (1999).
[9] R. K. Singh and J. Narayan, Phys. Rev. B **41**, 8843 (1990).
[10] J. Gonzalo, C. N. Afonso, and I. Madriaga, J. Appl. Phys. **81**, 951 (1997).
[11] T. Scharf and H. U. Krebs, Appl. Phys. A: Mater. Sci. Process. **75**, 551 (2002).
[12] R. F. Wood, J. N. Leboeuf, D. B. Geohegan, A. A. Puretzky, and K. R. Chen, Phys. Rev. B **58**, 1533 (1998).
[13] C. M. Rouleau, D. H. Lowndes, J. W. McCamy, J. D. Budai, D. B. Poker, D. B. Geohegan, A. A. Puretzky, and S. Zhu, Appl. Phys. Lett. **67**, 2445 (1995).
[14] K. R. Chen, T. C. King, J. H. Hess, J. N. Leboeuf, D. B. Geohegan, R. F. Wood, A. A. Puretzky, and J. M. Donato, Phys. Rev. B **60**, 8373 (1999).
[15] D. H. Blank, H. Hilgenkap, A. Brinkan, D. Mijatovic, G. Rijinders, and H. Rogalla, Appl. Phys. Lett. **79**, 394 (2001).
[16] G. Grassano, W. Ramadan, V. Ferrando, E. Bellingeri, D. Marré, C. Ferdeghini, G. Grasso, M. Putti, P. Manfrinetti, A. Palenzona, and A. Chincarini, Supercond. Sci. Technol. **14**, 762 (2001).
[17] J. Nagamatsu, N. Nakagawa, T. Muranaka, Y. Zenitani, and J. Akimitsu, Nature (London) **410**, 63 (2001).
[18] R. J. Cava, Nature (London) **410**, 23 (2001).
[19] Y. Tang and Q. Qin, Chem. Phys. Lett. **343**, 452 (2001).
[20] S. Amoruso, R. Bruzzese, N. Spinelli, R. Velotta, X. Wang, and C. Ferdeghini, Appl. Phys. Lett. **80**, 4315 (2002).
[21] Ya. B. Zel'dovich and Yu. P. Raizer, *Physics of Shock Waves and High-Temperature Hydrodynamic Phenomena* (Academic, New York, 1966).
[22] W. C. Martin, J. Sugar, A. Musgrove, G. R. Dalton, W. L. Wiese, J. R. Fuhr, and D. E. Kelleher, *NIST Database for Atomic Spectroscopy* (NIST, Gaithersburg, MD, 1995).
[23] P. R. Willmott and J. R. Huber, Rev. Mod. Phys. **72**, 315 (2000).
[24] W. D. Westwood, J. Vac. Sci. Technol. **15**, 1 (1978).
[25] D. B. Geohegan, Appl. Phys. Lett. **60**, 2732 (1992).
[26] P. E. Dyer, A. Issa, and P. H. Key, Appl. Phys. Lett. **57**, 186 (1990).

[27] M. Ohkoshi, Y. Yoshitake, and K. Tsushima, Appl. Phys. Lett. **64**, 3340 (1994).
[28] T. E. Itina, L. Patrone, W. Marine, and M. Autric, Appl. Phys. A: Mater. Sci. Process. **69**, S59 (1999).
[29] L. D. Landau and E. M. Lifschitz, *Fluid Mechanics* (Pergamon, Oxford, 1966).
[30] L. I. Sedov, *Similarity and Dimensional Methods in Mechanics* (CRC Press, Boca Raton, FL, 1993).
[31] S. I. Anisimov, D. Bäuerle, and B. S. Luk'yanchuk, Phys. Rev. B **48**, 12 076 (1993).
[32] N. Arnold, J. Gruber, and J. Heitz, Appl. Phys. A: Mater. Sci. Process. **69**, s87 (1999).
[33] A. Gupta, B. Braren, K. G. Casey, B. W. Hussey, and R. Kelly, Appl. Phys. Lett. **59**, 1302 (1991).
[34] J. T. Knudtson, W. B. Green, and D. G. Sutton, J. Appl. Phys. **61**, 4771 (1987).
[35] F. J. Gordillo-Vasquez, A. Perea, J. A. Chaos, J. Gonzalo, and C. N. Afonso, Appl. Phys. Lett. **78**, 7 (2001).
[36] R. J. Goldston and P. H. Rutherford, *Introduction to Plasma Physics* (Institute of Physics, London, 1995).